Heliyon

ELSEVIER

Received:
12 November 2018
Revised:
8 January 2019
Accepted:
25 January 2019

Cite as: Vladimir V. Popov, Alexander Katz-Demyanetz, Andrey Koptyug, Menachem Bamberger. Selective electron beam melting of Al0.5CrMoNbTa0.5 high entropy alloys using elemental powder blend. Heliyon 5 (2019) e01188. doi: 10.1016/j.heliyon.2019.e01188

Selective electron beam melting of Al0.5CrMoNbTa0.5 high entropy alloys using elemental powder blend

Vladimir V. Popov [a], **Alexander Katz-Demyanetz** [a,*], **Andrey Koptyug** [b], **Menachem Bamberger** [c]

[a] *Israel Institute of Metals, Technion R&D Foundation, Technion City, 3200003, Haifa, Israel*

[b] *Sports Tech Research Centre, Mid Sweden University, Akademigatan1, SE-831 25, Östersund, Sweden*

[c] *Department of Materials Science and Engineering, Technion – Israel Institute of Technology, Technion City, Haifa, 3200003, Israel*

[*] Corresponding author.

E-mail address: kalexand@technion.ac.il (A. Katz-Demyanetz).

Abstract

High Entropy Alloys (HEAs) is a novel promising class of multi-component materials which may demonstrate superior mechanical properties useful for high-temperature applications. Despite the high potential of HEAs, their production is complicated, using pre-alloyed powders in powder metallurgy route. This significantly complicates development and implementation of refractory BCC solid solution based HEAs. The present paper reports on experiments aiming at production of Al0.5CrMoNbTa0.5 multi-principle alloy using powder bed beam based additive manufacturing. Samples were manufactured using Selective Electron Beam Melting (SEBM) additive manufacturing technique from a blend of elemental powders aiming at achieving microstructure with high configurational entropy. Though it was not possible to achieve completely homogeneous microstructure, the as-printed material was composed of the zones with two multi-component solid solutions, which differed only by Al content confirming *in situ* alloying. The process parameters optimization was not carried out and the as-print material contained a notable amount of residual porosity. It

https://doi.org/10.1016/j.heliyon.2019.e01188

was possible to reach lower porosity level using heat treatment at 1300 °C for 24 hours, however undesirable alloy composition changes took place. The main conclusion is that the production of the Al0.5CrMoNbTa0.5 multi-principle alloy from elemental powder blends using SEBM technique is achievable, but the process parameter optimization rather than post-process heat treatment should be performed to reduce the porosity of samples.

Keywords: Materials science, Metallurgical engineering

1. Introduction

High Entropy Alloys (HEA) are a group of multi-component materials, in which formation of a single-phase solid solution (i.e. a phase with high configurational entropy) is preferable over the formation of intermetallic compounds [1, 2, 3]. Refractory metals containing HEAs usually have a microstructure based on multi-component solid solution with body centered cubic (BCC) microstructure [4, 5, 6, 7, 8, 9, 10]. They demonstrate increased high-temperature mechanical strength, thus showing a high potential to improve the presently existing alloys containing critical elements currently exploited at high temperatures [4, 5, 6, 7, 8, 9, 10]. In order to decrease the specific weight of the alloy, full or partial substitution of W, Mo and Ta by transition metals [6, 7, 8, 9, 10] and even by Al [11] was proposed and successfully tested.

The conventional way to produce HEAs is a vacuum arc melting [8, 9, 12, 13, 14]. In this production route, the alloying constituents are heated in vacuum up to a temperature higher than their melting point and then mixed in the liquid state. After the mixing is complete the as-obtained liquid is solidified and then heat treated, if it is necessary for homogenization required for achieving desired mechanical properties. The main problem of such route is the difference in melting points and vapor pressures of the alloying elements at high temperatures. Furthermore, if the produced HEA is a refractory alloy and, therefore, the melting points of the alloying elements are significantly high, the castability of such liquid blend in insufficient to obtain a homogeneous material. Additionally, oxidation resistance of refractory metals is insufficient to obtain non-oxidized product even under operating vacuum typical for high temperature arc-melting. Taking into account the mentioned problematic aspects, it becomes clear that more appropriate HEA production route should be developed, especially for the HEAs containing refractory constituents.

Powder Bed Additive Manufacturing (PB-AM) is one of the potential new routes for HEAs production. Extremely fast melting and solidification of material in inert atmosphere or in vacuum (as with SEBM) together with the freedom of component

https://doi.org/10.1016/j.heliyon.2019.e01188

shapes suggest that this route could be used even for the HEAs containing elements with low oxidation resistance and poor castability.

Traditionally powder bed additive manufacturing uses pre-alloyed powders. If for some material compositions homogeneous alloying is complicated or is not possible, such powders would be not available or prohibitively expensive despite the availability of various methods for their production. Essentially, at the earliest stages of powder production all problems showing up in the common HEA manufacturing routes will be present. Low availability of the pre-alloyed powders for new perspective materials is one of the factors slowing the development of powder bed AM in general and PB-AM of refractory metallic materials in particular. Though the interest in the development of new materials for PB-AM is continuously increasing, to the moment the number of literature sources reporting on the trials for *in-situ* alloying in PB-AM aiming at high entropy alloys is very small.

Ocelik et al. [15] reported that PB-AM of HEAs from elemental powders is achievable by laser processing. The authors mentioned that solidification rate is a critical parameter for successful HEA manufacturing, and that is why high power laser beam with regulated density and speed is a unique benefit of PB-AM. However, the samples demonstrated in this work were three-layered coatings, not bulk specimens. It is obvious that the PB-AM process optimization for manufacturing of homogeneous structured HEAs using this approach requires further development.

X. Li [16] considered the prospects of AM route for the production of Bulk Metallic Glasses (BMG) and HEAs. One of the presented possible approaches for HEAs fabrication is Selective Laser Melting (SLM). It is also noted that SLM of blended powders can be used for HEAs manufacturing. However, in this paper or in the previous publications by the same author no confirmation on the successful results in PB-AM of HEAs from elemental powders is given. These publications are mostly devoted to the manufacturing of advanced composite alloys from the blends of pre-alloyed powders.

Chao et al. [17] announced progress in direct laser manufacturing of bulk HEAs from blended elemental powders [17]. However only the conference abstract of this work with no mechanical, thermal or microstructural results is available.

Publications [18, 19, 20] present the findings on the SLM of pre-alloyed HEA powders. The results confirm the possibility of laser melting in producing bulk HEA parts.

Haase et al. [21] performed successful experiments and simulation of SLM of HEA from a blend of elemental powders. The authors concluded that such approach is very attractive because of easy modifying of powder composition. HEAs produced

https://doi.org/10.1016/j.heliyon.2019.e01188

by this way demonstrated relatively high strength and homogeneous composition. The authors also noted the importance of proper adjustment of the laser beam power for homogeneity of the final PB-AM manufactured components. According to the literature survey and findings presented in this paper, the mechanical strength of AM-manufactured HEAs is higher compared to the traditionally manufactured ones (casting).

The relatively wide range of works on the laser-based PB AM of HEAs can be explained by a large amount of different available laser based AM machines and significant research activities aiming at introducing new materials for them, complementing to a rather wide range of the already existing ones. Selective Electron Beam Melting (SEBM) machines so far are commercially manufactured only by ARCAM EBM [22], and there is only a very limited number of commercially available materials. SEBM process has unique benefits, such as vacuum environment and high temperature process conditions. These factors provide high quality of manufactured metal alloys with reduced residual stress and low porosity level.

There are already several papers [23, 24, 25, 26, 27, 28] describing potential advantages of SEBM for HEAs production, but all describe experiments with pre-alloyed powders. In general, the loss of the alloying elements due to the uneven evaporation can be more significant in the SEBM as compared to the laser-based PB AM due to the higher beam power.

Cui et al. [29] reviewed and discussed a thermodynamic approach predicting stability of HEAs and gave a number of examples for successful attempts of laser-based additive manufacturing of these multi-component alloys from blended elemental Al, Co, Cr, Fe, Ni and Cu powders.

Dobbelstein et al. [30] reported on direct metal deposition of refractory MoNbTaW HEA. The authors discussed the used experimental set-up which permitted to perform *in-situ* alloying of the pre-mixed powder blend. Effect of the process parameters on a product oxidation and on the obtained microstructure and mechanical properties is discussed.

Joseph et al. [31] compared microstructure and mechanical properties of the direct laser fabricated (DLF) and arc-melted $Al_xCoCrFeNi$ HEA. The authors described in detail both the process and the effect of the production parameters on phase formation, undesirable oxidation and mechanical properties of the resulting material. The main conclusion is that the DLF production route permits to obtain materials with the microstructure and properties similar to those obtained by a conventional arc-melting.

No reports on attempts to produce HEAs from elemental powders using selective electron beam melting (SEBM) were found in the literature.

https://doi.org/10.1016/j.heliyon.2019.e01188

2. Materials and methods

The samples were manufactured from the blend of powders at Sports Tech Research Centre, Mid Sweden University in the ARCAM EBM A2 machine (by ARCAM EBM, a GE Additive Company, Göteborg, Sweden) modified for manufacturing of test samples from small powder batches. Modified setup uses small working area with the base plate diameter 82 mm and small powder container connected to the raking mechanism (see [32] for details). Vertical arrangement of the powder container allows for working with small amounts of powder (down to 100 cm^3). Extensive trials with this setup confirmed that such arrangement allows working with powders having rather restricted flow ability, with powder blends where the main powder fraction has good flow ability and relatively coarse grains (e.g. having powder distribution close to 75−150 μm) and the other (minor) fractions are relatively fine, and also working with the blends of powders with irregular grains having wide powder grain size distributions.

SEBM manufacturing was carried out with 920 °C target working temperature of the build and layer thickness set to 50 μm. The melting was carried out with the hatch changing direction 90° each next layer and beam speed of 80 mm/s and beam current of 20 mA (energy density 15 J/mm). Outer surfaces of the samples are defined by standard double contours in ARCAM 'multi-beam' settings. Given parameter settings were not optimized but allowed for manufacturing of solid test samples with acceptable quality.

Fig. 1 presents the used elemental powders and the powder blend prepared using their mechanical mixing by tumbling in a glass jar for 40 minutes. The powders have been examined by SEM/EPMA to confirm the prepared blend homogeneity.

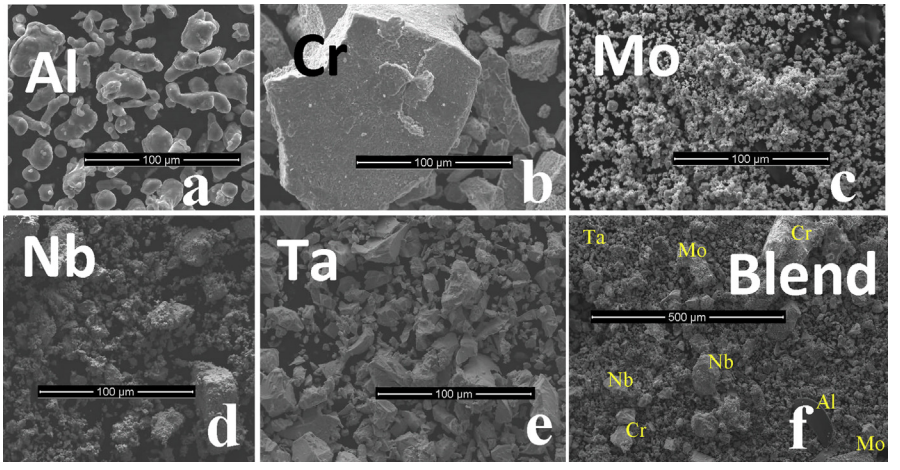

Fig. 1. Secondary Electron images of elemental powders and final blended Al0.5CrMoNbTa0.5 powder. a − Aluminum powder; b − Chromium powder; c − Molybdenum powder; d − Niobium powder; e − Ta − Tantalum powder; f − powders blend.

https://doi.org/10.1016/j.heliyon.2019.e01188

Table 1. Characteristics of powders.

Powder	Purity, %	Fraction, μm	Supplier
Aluminum	99.0	200 mesh/74 μm	ACROS Organics
Chromium	99.0	−100 mesh/149 μm	Strem Chemicals, Inc.
Niobium	99.8	−325 mesh/44 μm	Strem Chemicals, Inc.
Tantalum	99.8	−325 mesh/44 μm	Strem Chemicals, Inc.
Molybdenum	99.9	3−7	Strem Chemicals, Inc.

The powders' characteristics are presented in Table 1. The blend calculation is presented in Table 2. From Fig. 1 it is clear that elemental powders have different particle size distributions and morphology, and all are far from what is traditionally used in commercial PB AM machines. Though all elemental powders have quite low flow ability, it was possible to work with them using modified powder delivery system with vertical powder container [32, 33, 34].

Heat treatment aimed at microstructural homogenization was performed for 24 hours in vacuumed quartz ampules under two different conditions: at 1000 and at 1300 °C.

For the microstructure examination the as-manufactured and heat treated samples were cut and polished using paper and several types of emulsion. For the analysis Scanning Electron Microscope SEM FEI Inspect (FEI, Brno, Czech Republic) equipped with Electron Probe Micro Analyzer (EPMA) was employed. Back-Scattered Electrons Detector was used to obtain phase contrast. Accelerating voltage used was 20 kV; working distance was approximately 9 ÷ 11 mm.

The phase content of SEBM as-manufactured and heat-treated samples was examined by X-ray diffraction in Rigaku SmartLab 9-KW diffractometer with Cu X-ray tube (Rigaku, Tokyo, Japan). The scattering range was 20−80°, the scan increment was 0.1° and scan speed was 1°/min.

Table 2. Calculation of $Al_{0.5}Cr_{1.0}Mo_{1.0}Nb_{1.0}Ta_{0.5}$ powder blend per total volume 300 ml.

Element	Molar %	Molar weight, g/mole	Density, g/cm^3	Volume %	Volume per overall volume 300 cm^3, cm^3	Weight per overall volume 300 cm^3, g
Al	12	26,98	2,69	12.66	38.0	102
Cr	25	52,00	7,19	19,09	57.3	412
Mo	25	95,94	10,22	24,79	74,4	760
Nb	25	92,91	8,57	28,59	85,7	734
Ta	13	180,95	16,65	14,87	44.6	743
	100			**100,00**	**300,0**	**2751**

https://doi.org/10.1016/j.heliyon.2019.e01188

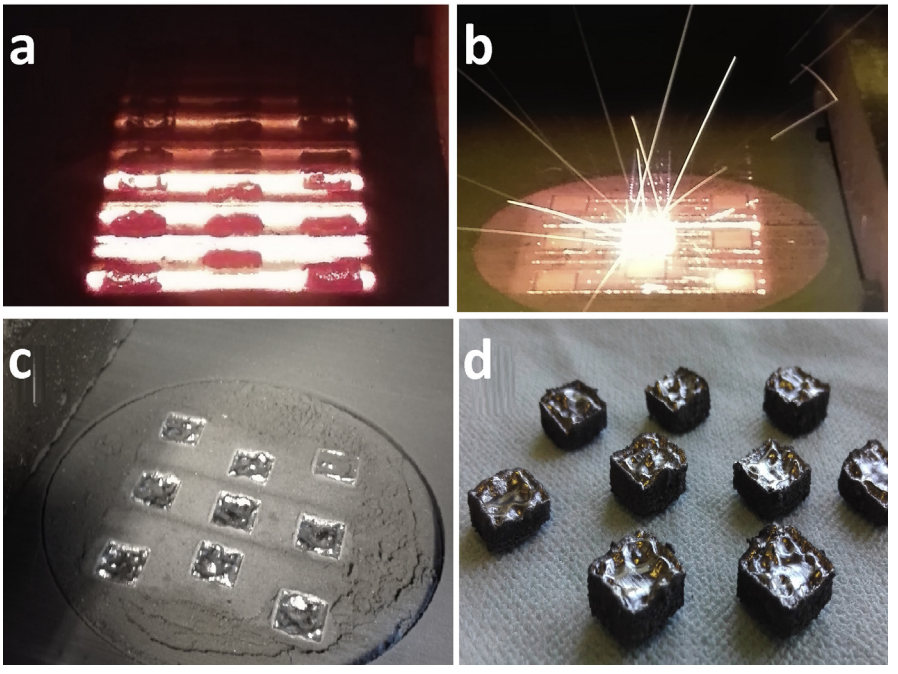

Fig. 2. Production chain: a – powder semi-sintering in each layer; b – melting of the samples in each layer; c – manufactured bulk samples sounded by the semi-sintered powder; d – bulk samples removed from the base plate.

3. Results

The sample manufacturing process is illustrated in Fig. 2. Powders blend is prepared and loaded into the powder delivery system. CAD file for the build in the corresponding format is loaded and desired machine parameters are set. Base plate is heated up to the working temperature and layer-by-layer manufacturing process is initiated. Before the melting in each layer is conducted, the powder

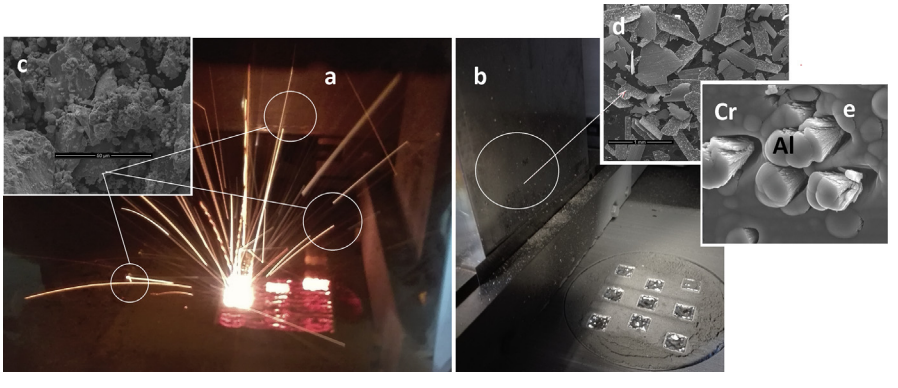

Fig. 3. Powder loss during SEBM process: a – "fireworks" – powder removed from the powder bed by high power electron beam; b – metalized surface of the powder hopper and rake after SEBM process; c – SEM-image of the powder lost by "fireworks"; d–e – SEM-images of the metallization flakes in different magnifications.

https://doi.org/10.1016/j.heliyon.2019.e01188

should be semi-sintered (Fig. 2a). Loose powder is charged by electron beam and can form a cloud in the vacuum chamber, which stops the process and is potentially damaging for the machine. Thus semi-sintering of the powder layer is carried out with the de-focused e-beam in steps with successively increasing power. Full power of the sharply focused beam now can be applied to melt the layer areas where the solid parts of the manufactured components are located (Fig. 2b). Two-stage preheat-melt process of SEBM results in manufactured components being surrounded by semi-sintered powder (Fig. 2c) that should

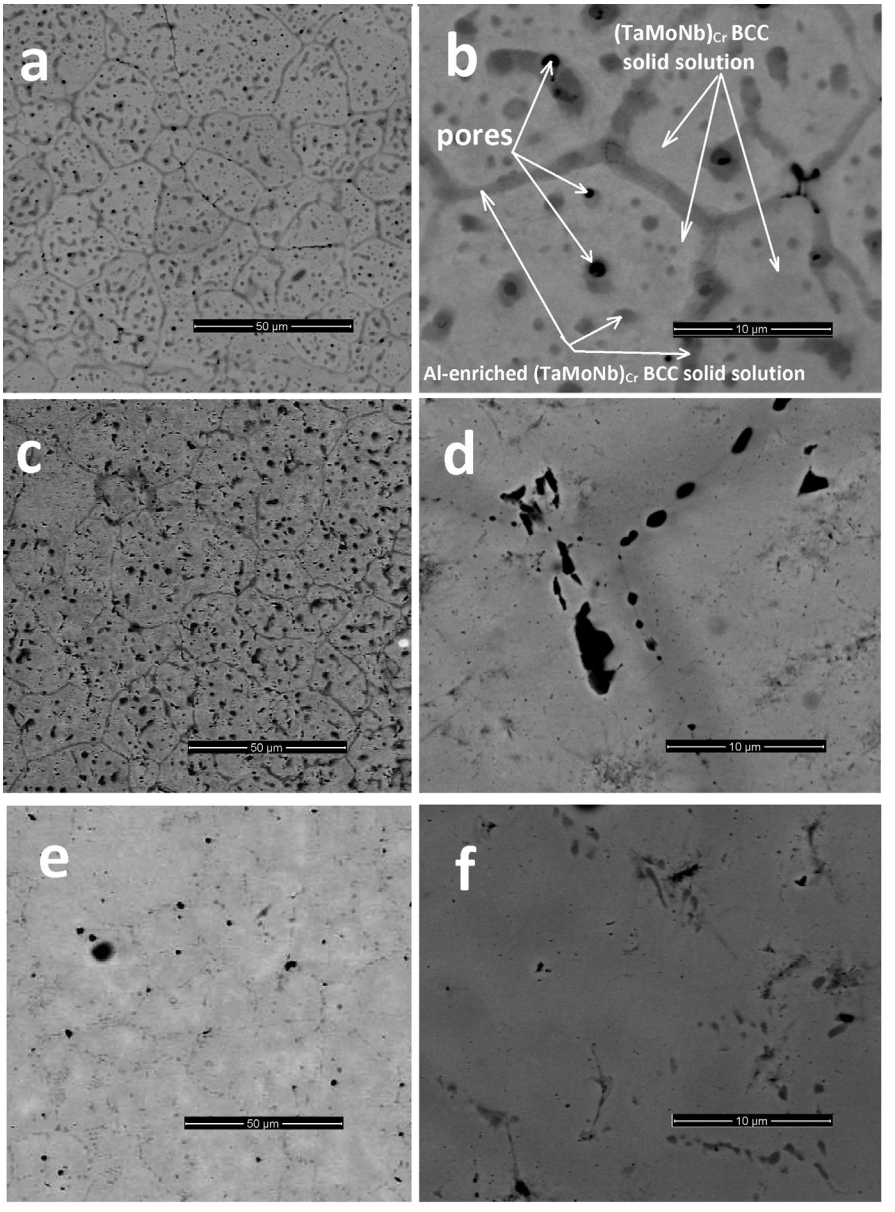

Fig. 4. Typical microstructures of the as-manufactured (a, b) and heat-treated samples at 1000 °C (c, d); and at 1300 °C (e, f).

https://doi.org/10.1016/j.heliyon.2019.e01188

be removed and can be returned to further manufacturing. Samples are further removed from the base plate (Fig. 2d).

Fig. 3 presents a typical view of the melting process through the SEBM machine inspection window (Fig. 3a), and the presence of large amount of material splatter is clearly visible (see Fig. 3a–e).

Typical microstructure of as-manufactured alloy samples is illustrated in Fig. 4.

Chemical compositions of the overall initial powder, as-built and heat-treated samples and different phases revealed by SEM have been measured by SEM/EMPA and are listed in Table 3.

X-ray diffraction spectra of as-manufactured and heat-treated samples are presented in Fig. 5.

4. Discussion

The presence of the splatter ("fireworks") seen in Fig. 3a is common for all powder based AM melting processes and is most probably caused by the instabilities in the melt pool dynamics and high metal vapor pressure [35, 36, 37, 38]. In SEBM this splatter is significantly more pronounced when working with the powders having small particle size. When working with powder blends together with uneven evaporation of different elements it can affect the composition and homogeneity of the resulting material. Evaporation temperatures of the elements composing the examined powders blend are given in Table 4 [39]. It can be seen that through the printing process, when the operating vacuum is approximately 10^{-3} mbar and the temperature of electron beam molten metal pool may achieve 2500 °C, the obtaining of the desired chemical composition of a product is a technological challenge. The problem

Table 3. Chemical composition of different phases of the as-manufactured samples in comparison to the initial powder.

Sample	Phase description	Element content, at. %				
		Al	Cr	Mo	Nb	Ta
Initial powder	Overall	12.0	25.0	25.0	25.0	13.0
As-built	Overall	8.4	25.8	25.7	26.5	13.6
	TaMoNbCr s.s.	1.4	9.4	39.1	29.9	20.2
	$(TaMoNbCr)_{Al}$ s.s.	11.8	27.6	24.8	24.3	11.5
HT 1000 °C	Overall	8.0	24.7	26.3	26.4	14.6
	TaMoNbCr s.s.	1.3	9.3	38.7	29.7	21.0
	$(TaMoNbCr)_{Al}$ s.s.	11.7	27.4	24.3	24.2	12.4
HT 1300 °C	Overall	7.8	23.2	26.7	27.3	15.0
	TaMoNbCr s.s.	1.3	9.9	37.5	30.9	20.4
	$(TaMoNbCr)_{Al}$ s.s.	11.8	28.5	23.4	23.8	12.5

https://doi.org/10.1016/j.heliyon.2019.e01188

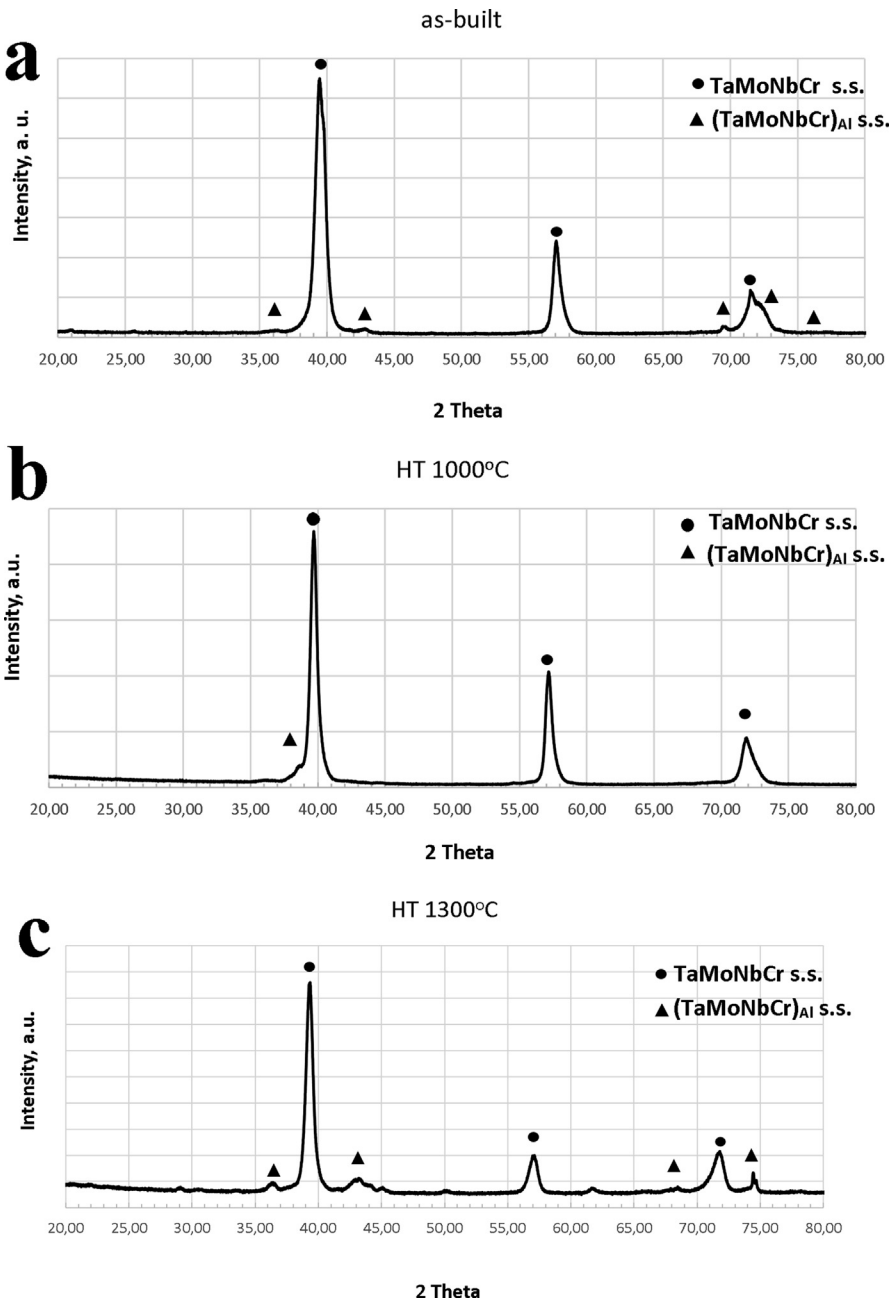

Fig. 5. XRD spectra of the as-manufactured and post-heat-treated samples. a – as-manufactured sample; b – sample heat treated at 1000 °C; c – sample heat treated at 1300 °C.

of possible evaporation of light metals may be overcome only by addition of excess amount of them to the initial powders blend.

Crust forming on the metal shields surrounding the melt zone containing the result of metal vapor condensation with embedded freezing splatter droplets of Al in Cr-matrix (according to SEM/EPMA) has been revealed (see Fig. 3b).

https://doi.org/10.1016/j.heliyon.2019.e01188

Table 4. Evaporation temperatures of the elements composing the examined powders blend under different pressures [39].

Element	Evaporation temperatures at different pressures, °C		
	At 10^{-2} mbar	At 10^{-3} mbar	At 10^{-4} mbar
Al	1209	1087	982
Cr	1383	1254	1144
Mo	2466	2258	2080
Nb	2669	2439	2256
Ta	3025	2776	2567

EPMA analysis shows that an average chemical composition of the splatter droplets is close to that of the blended powder and includes all five elements, and thus "fireworks" should not have significant influence on the resulting material composition of the solid samples. Structures resulting from the metal vapor condensation are relatively easily distinguished on the screen surface and the embedded splatter droplets, commonly having the appearance of loose or packed "needles". EPMA analysis of these structures indicates that aluminum and chromium are predominantly evaporating from the melt put in our case (see Fig. 3d–e).

It can be seen from Table 3 that a notable amount of Al evaporated through the printing process: the as-built sample contains only 8.4 at % Al instead of the designed 12.0 at %. Through the after-printing vacuum heat treatments, slight depletion of Al and Cr was revealed: the sample heat treated at 1000 °C contained only 8.0 at % Al and 24.7 at % Cr as against 8.4 and 25.8 at % measured in the as-built sample, respectively. Heat treatment at 1300 °C caused additional decrease in overall Al and Cr content: 7.8 at % Al and 23.2 at % Cr. The observed decrease in Al and Cr content through heat treatment is caused by the alloy depletion of these elements in the environment of a vacuum in the ampules (see Table 4).

It can be seen (Fig. 4a–b) that the microstructure of the as-manufactured sample consists of two phases distinguished in BSE image as bright and dark areas corresponding to TaMoNbCr and $(TaMoNbCr)_{Al}$ solid solutions, respectively. Chemical microanalysis results are shown in Table 4. Considering these findings together with XRD spectrum obtained from this sample (Fig. 5a), it becomes clear that two different solid solutions formed through SEBM manufacturing of the sample: rich and poor in Al. The Al-poor phase is based on BCC TaNbMo solid solution (according to XRD), while the majority of Al is located in Al-rich grain boundary and in-grain second-phase solid solution phases. As it can be seen from Fig. 4c,d, post-manufacturing heat treatment at 1000 °C caused slight decrease in the amount of

https://doi.org/10.1016/j.heliyon.2019.e01188

Al-rich phase. Fig. 4e–f illustrate the microstructure formed after post-manufacturing heat treatment at 1300 °C. Significant residual porosity is observed in all examined samples.

5. Conclusions

1. Selective Electron Beam Melting (SEBM) powder bed beam based additive manufacturing (AM) technology was used for preparation of $Al_{0.5}Cr_{1.0}Mo_{1.0}Nb_{1.0}Ta_{0.5}$ multi-principle alloy from a blend of elemental powders.
2. Despite a notable Al evaporation occurred through the alloy's manufacturing, the *in situ* alloying of five-elemental powders has been confirmed by the microstructural examination of the as-built sample.
3. According by SEM/EPMA observation and XRD examination, the obtained microstructure of as-manufactured samples is composed of two solid solutions: matrix phase corresponding to TaMoNb-based solid solution with low (1.4 at. %) Al content, and second (minor) phase corresponding to $(TaMoNbCr)_{Al}$ solid solution with relatively high (~11.8 at. %) Al content. The as-manufactured samples contained a significant amount of residual porosity, most probably due to the process parameter settings being far from optimal.
4. The post-manufacturing heat treatments performed in vacuumed ampules at various temperatures improved the microstructural homogenization of the as-printed samples, but did not affect the residual porosity.
5. In general, the results obtained illustrate that elemental powder blends can be used for SEBM manufacturing of high entropy alloys. The results of the performed trials of SEBM manufacturing of $Al_{0.5}Cr_{1.0}Mo_{1.0}Nb_{1.0}Ta_{0.5}$ multi-principle alloy with high potential to form a microstructure with high configurational entropy (i.e. multi-component single-phase solid solution) are quite promising, and show that *in-situ* alloying of elemental powders for HEAs manufacturing is achievable.

Declarations

Author contribution statement

Vladimir V. Popov: Conceived and designed the experiments; Performed the experiments; Wrote the paper.

Alexander Katz-Demyanetz: Conceived and designed the experiments; Analyzed and interpreted the data; Wrote the paper.

Andrey Koptyug: Performed the experiments; Wrote the paper.

https://doi.org/10.1016/j.heliyon.2019.e01188

Menachem S. Bamberger: Analyzed and interpreted the data; Contributed reagents, materials, analysis tools or data; Wrote the paper.

Funding statement

This research did not receive any specific grant from funding agencies in the public, commercial, or not-for-profit sectors.

Competing interest statement

The authors declare no conflict of interest.

Additional information

No additional information is available for this paper.

References

[1] J.W. Yeh, S.K. Chen, S.J. Lin, J.Y. Gan, T.S. Chin, T.T. Shun, C.H. Tsau, S.Y. Chang, Nanostructured High-Entropy Alloys with Multiple Principal Elements: Novel Alloy Design Concepts and Outcomes, 2004.

[2] Y.P. Wang, B.S. Li, H.Z. Fu, Solid solution or intermetallics in a high-entropy alloy, Adv. Eng. Mater. 11 (2009) 641−644.

[3] Y. Zhang, X. Yang, P.K. Liaw, Alloy design and properties optimization of high-entropy alloys, JOM 64 (7) (2012) 830−838.

[4] O.N. Senkov, G.B. Wilks, J.M. Scott, D.B. Miracle, Mechanical properties of Nb25Mo25Ta25W25 and V20Nb20Mo20Ta20W20 refractory high entropy alloys, Intermetallics 19 (2011) 698−706.

[5] O.N. Senkov, J.M. Scott, S.V. Senkova, Microstructure and room temperature properties of a high entropy TaNbHfZrTi alloy, in: D.B. Miracle, C.F. Woodward (Eds.), Metals Branch Metals, Ceramics and NDE Division, AFRL-RX-WP-TP-2011-4292UES, Inc, 2011.

[6] O.N. Senkov, S.V. Senkova, C.F. Woodward, D.B. Miracle, Low-density, refractory multi-principal element alloys of the Cr−Nb−Ti−V−Zr system: microstructure and phase analysis, Acta Mater. 61 (2013) 1545−1557.

[7] O.N. Senkov, C.F. Woodward, Microstructure and properties of a refractory NbCrMo0.5Ta0.5TiZr alloy, Mater. Sci. Eng. A 529 (1) (2011) 311−320.

https://doi.org/10.1016/j.heliyon.2019.e01188

[8] O.N. Senkov, J.M. Scott, S.V. Senkova, F. Meisenkothen, D.B. Miracle, C.F. Woodward, Microstructure and elevated temperature properties of a refractory TaNbHfZrTi alloy, J. Mater. Sci. 47 (2012) 4062−4074.

[9] O.N. Senkov, J.M. Scott, S.V. Senkova, D.B. Miracle, C.F. Woodward, Microstructure and room temperature properties of a high-entropy TaNbHfZrTi alloy, J. Alloys Compd. 509 (2011) 6043−6048.

[10] O.N. Senkov, S.L. Semiatin, Microstructure and properties of a refractory high-entropy alloy after cold working, J. Alloys Compd. 649 (2015) 1110−1123.

[11] O.N. Senkov, S.V. Senkova, F. Woodward, Effect of aluminum on the microstructure and properties of two refractory high-entropy alloys, Acta Mater. 68 (2014) 214−228.

[12] N. Larianovsky, A. Katz-Demyanetz, E. Eshed, M. Regev, Microstructure, tensile and creep properties of Ta20Nb20Hf20Zr20Ti20 high entropy alloy, Materials 10 (2017) 883.

[13] E. Eshed, N. Larianovsky, A. Kovalevsky, V. Popov Jr., I. Gorbachev, V. Popov, A. Katz-Demyanetz, Microstructural evolution and phase formation in 2nd-generation refractory-based high entropy alloys, Materials 11 (2018) 75.

[14] E. Eshed, N. Larianovsky, A. Kovalevsky, A. Katz-Demyanetz, Effect of Zr on the microstructure of second- and third-generation BCC HEAs, JOM Miner. Metals Mater. Soc. (2018).

[15] V. Ocelik, N. Janssen, S.N. Smith, J. Th. M. De Hosson, Additive manufacturing of high-entropy alloys by laser processing, JOM 68 (2016).

[16] X. Li, Additive manufacturing of advanced multi-component alloys: bulk metallic glasses and high entropy alloys, Adv. Eng. Mater. 20 (2018) 1700874.

[17] Q. Chao, J. Joseph, P. Hodgson, D. Fabijanic, Direct Laser Manufactured High Entropy Alloys, IWHEM-2017 Digest book, 2017, p. 24.

[18] R. Zhou, Y. Liu, C. Zhou, S. Li, W. Wu, M. Song, B. Liu, X. Liang, P.K. Liaw, Microstructures and mechanical properties of C-containing FeCoCrNi high-entropy alloy fabricated by selective laser melting, Intermetallics 94 (2018) 165−171.

[19] Z.G. Zhu, Q.B. Nguyen, F.L. Ng, X.H. An, X.Z. Liao, P.K. Liaw, S.M.L. Nai, J. Wei, Hierarchical microstructure and strengthening mechanisms of a

 https://doi.org/10.1016/j.heliyon.2019.e01188

CoCrFeNiMn high entropy alloy additively manufactured by selective laser melting, Scr. Mater. 154 (2018) 20–24.

[20] Y. Brif, M. Thomas, I. Todd, The use of high-entropy alloys in additive manufacturing, Scr. Mater. 99 (2015) 93–96.

[21] C. Haase, F. Tang, M.B. Wilms, A. Weisheit, B. Hallstedt, Combining thermodynamic modeling and 3D printing of elemental powder blends for high-throughput investigation of high-entropy alloys – towards rapid alloy screening and design, Mater. Sci. Eng. A 688 (2017) 180–189.

[22] ARCAM EBM, a GE additive company; Company web site: http://www.arcam.com/.

[23] S.-H. Sun, Y. Koizumi, S. Kurosu, Y.-P. Li, H. Matsumoto, A. Chiba, Build direction dependence of microstructure and high-temperature tensile property of Co–Cr–Mo alloy fabricated by electron beam melting, Acta Mater. 64 (2014) 154–168.

[24] R. Dehoff, M. Kirka, W.J. Sames, H. Bilheux, A. Tremsin, L. Lowe, S. Babu, Site specific control of crystallographic grain orientation through electron beam additive manufacturing, Mater. Sci. Technol. 31 (2014).

[25] T. Fujieda, H. Shiratori, K. Kuwabara, T. Kato, K. Yamanaka, Y. Koizumi, A. Chiba, First demonstration of promising selective electron beam melting method for utilizing high-entropy alloys as engineering materials, Mater. Lett. 159 (2015) 12–15.

[26] T. Fujieda, H. Shiratori, K. Kuwabara, M. Hirota, T. Kato, K. Yamanaka, Y. Koizumi, A. Chiba, S. Watanabe, CoCrFeNiTi-based high-entropy alloy with superior tensile strength and corrosion resistance achieved by a combination of additive manufacturing using selective electron beam melting and solution treatment, Mater. Lett. 189 (2017) 148–151.

[27] H. Shiratori, T. Fujieda, K. Yamanaka, Y. Koizumi, K. Kuwabara, T. Kato, A. Chiba, Relationship between the microstructure and mechanical properties of an equiatomic AlCoCrFeNi high-entropy alloy fabricated by selective electron beam melting, Mater. Sci. Eng. A 656 (2016) 39–46.

[28] K. Kuwabara, H. Shiratori, T. Fujieda, K. Yamanaka, Y. Koizumi, A. Chiba, Mechanical and corrosion properties of AlCoCrFeNi high-entropy alloy fabricated with selective electron beam melting, Addit. Manuf. 23 (2018) 264–271.

[29] W. Cui, X. Zhang, F. Liou, Additive manufacturing of high-entropy alloys – a review, solid freeform fabrication 2017, in: Proceedings of the 28th Annual

 https://doi.org/10.1016/j.heliyon.2019.e01188

International Solid Freeform Fabrication Symposium – An Additive Manufacturing Conference, 2017, pp. 712–724.

[30] H. Dobbelstein, M. Thiele, E.L. Gurevich, E.P. George, A. Ostendorf, Direct metal deposition of refractory high entropy alloy MoNbTaW, Phys. Proc. 83 (2016) 624–633.

[31] J. Joseph, T. Jarvis, X. Wu, N. Stanford, P. Hodgson, D.M. Fabijanic, Comparative study of the microstructures and mechanical properties of direct laser fabricated and arc-melted AlxCoCrFeNi high entropy alloys, Mater. Sci. Eng. A 633 (2015) 184–193.

[32] A. Koptyug, L.-E. Rännar, C. Botero, M. Bäckström, V. Popov, Blended powders can be successfully used in Electron Beam Melting yielding unique material compositions, in: EuroPM2018 Proceedings, EPMA, 2018 (out electronically).

[33] A. Koptyug, M. Bäckström, C. Botero, V. Popov, E. Chudinova, Developing new materials for electron beam melting: experiences and challenges, Mater. Sci. Forum 941 (2018) 2190–2195.

[34] V. Popov, A. Koptyug, I. Radulov, F. Maccari, G. Muller, Prospects of additive manufacturing of rare-earth and non-rare-earth permanent magnets, Proc. Manuf. 21 (2018) 100–108.

[35] C. Lun, A. Leung, S. Marussi, R.C. Atwood, M. Towrie, P.J. Withers, P.D. Lee, In situ X-ray imaging of defect and molten pool dynamics in laser additive manufacturing, Nat. Commun. 9 (2018). Article number: 1355.

[36] S.A. Khairallah, A.T. Anderson, A. Rubenchik, W.E. King, Laser powder-bed fusion additive manufacturing: physics of complex melt flow and formation mechanisms of pores, spatter, and denudation zones, Acta Mater. 108 (2016) 36–45.

[37] M. Miyagi, H. Wang, R. Yoshida, Y. Kawahito, H. Kawakami, T. Shoubu, Effect of alloy element on weld pool dynamics in laser welding of aluminum alloys, Sci. Rep. 8 (2018). Article number: 12944.

[38] V. Popov, A. Katz-Demyanetz, M. Bamberger, Heat transfer and phase formation through EBM 3D-printing of Ti-6Al-4V cylindrical parts, Defect Diffus. Forum 383 (2018) 190–195.

[39] D. Stull, in: D.E. Gray (Ed.), American Institute of Physics Handbook, third ed., McGraw Hill, New York, 1972.

 https://doi.org/10.1016/j.heliyon.2019.e01188